Analysis of flexural wave cloaks

Alfonso Climente,[1,a] Daniel Torrent,[2,b] and José Sánchez-Dehesa[1,c]
[1]*Wave Phenomena Group, Department of Electronic Engineering, Universitat Politècnica de València, Camino de Vera s.n. (Building 7F), ES-46022 Valencia, Spain*
[2]*Universite de Bordeaux-Centre de Recherche Paul Pascal (CRPP, CNRS UPR 8641), 115 Avenue du Docteur Albert Schweitzer, 33600 Pessac, France*

(Received 28 June 2016; accepted 27 October 2016; published online 2 December 2016)

This work presents a comprehensive study of the cloak for bending waves theoretically proposed by Farhat *et al.* [see Phys. Rev. Lett. 103, 024301 (2009)] and later on experimentally realized by Stenger *et al.* [see Phys. Rev. Lett. **108**, 014301 (2012)]. This study uses a semi-analytical approach, the multilayer scattering method, which is based in the Kirchoff-Love wave equation for flexural waves in thin plates. Our approach was unable to reproduce the predicted behavior of the theoretically proposed cloak. This disagreement is here explained in terms of the simplified wave equation employed in the cloak design, which employed unusual boundary conditions for the cloaking shell. However, our approach reproduces fairly well the measured displacement maps for the fabricated cloak, indicating the validity of our approach. Also, the cloak quality has been here analyzed using the so called averaged visibility and the scattering cross section. The results obtained from both analysis let us to conclude that there is room for further improvements of this type of flexural wave cloak by using better design procedures. [http://dx.doi.org/10.1063/1.4968611]

I. INTRODUCTION

Acoustic cloaks based on two-dimensional (2D) anisotropic fluids were proposed by Cummer and Shurig[1,2] as an application of the transformation technique introduced earlier in designing 2D electromagnetic (EM) cloaks. Later, it was demonstrated that three-dimensional (3D) cloaks are also possible if one find the manner of engineering the acoustic properties of the anisotropic fluids designed for 3D cloaking. A route to engineer such kind of unusual fluids was opened by Torrent and Sánchez-Dehesa[3] and Cheng *et al.*,[4] who applied the metamaterial concept to design anisotropic fluid cloaks consisting of a multilayered structure of two isotropic and inhomogeneous fluids. In spite of the recent experimental realizations of anisotropic fluids, a clear demonstration of acoustic cloaks based on transformation acoustic is still lacking. However, acoustic cloaks based on scattering cancellation have been also proposed,[5–8] but the ones experimentally demonstrated have the drawbacks of being narrow banded and axisymmetric[6,7]

In parallel, the case of flexural wave cloaks was tackled by Farhat *et al.*[9] by using a simplified version of the Kirchoff-Love wave equation for thin plates. By applying a transformation technique they designed a cloak for bending waves consisting of a cylindrical shell made of an anisotropic elastic material confined between an outer radius b and an inner radius a. The purpose of such a shell was cloaking clamped objects with radius $R < a$, as it is schematically shown in Fig. 1. Later on, the same authors[10] designed another shell through homogenization of a multilayered concentric coating filled with piecewise constant isotropic elastic material. The last proposal was followed by

[a]alclial@upv.es
[b]torrent@crpp-bordeaux.cnrs.fr
[c]jsdehesa@upv.es

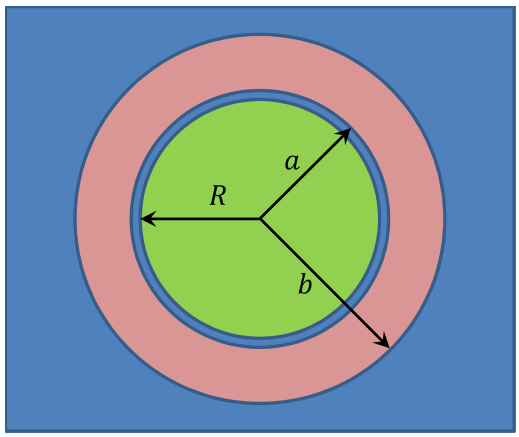

FIG. 1. Scheme of the flexural wave cloak for thin plates. The core (green area) with radius R defines the clamped object that is cloaked by the shell (pink area) with inner radius a and outer radius b. The separation (blue area) between the core and the cloak has the properties of the surrounding background.

Stenger *et al.*,[11] who introduced a further development in order to make the cloak feasible. Particularly, they fabricated metamaterial layers consisting of a composite of two polymers, a PVC plate with PDMS inclusions. Then, upon changing the filling fraction of the PDMS inclusion they were able to tailor the properties of the concentric layers forming the cloak.

This work comprehensibly analyzes the reported theoretical proposals as well as the experimental realization of the flexural wave cloaks. Our model approach employs a one dimensional multilayer scattering method (MLSM), which has been already applied in designing a wide variety of devices for flexural waves.[12–14] It is shown that our approach is unable to reproduce the working performance of the cloak reported by Farhat et al.,[9,10] however our MLSM reproduces fairly well the experimental data reported by Stenger et al.[11] From the analysis of the theoretically proposed cloaks we have concluded that they were obtained from an oversimplified wave equation which, additionally, does not verify the usual boundary conditions at the interface between the cloak and the surrounding background. Regarding the experimentally realized cloak, whose behavior is perfectly reproduced by the MLSM, its quality performance has been characterized with the so called averaged visibility parameter, γ, which gives in a single value the quality performance of the cloak in spatial regions near the cloak. The results obtained with this parameter have been compared with the results obtained for the scattering cross section, which characterizes the cloaking behavior at the far field. We have concluded that, in comparison with other reported cloaks, the performance of the flexural cloak could be substantially improved. Therefore, it is expected that cloaks for flexural waves with enhanced performance will be proven in the near future by introducing better design theories.[15]

This article is organized as follows. After this introduction, Sect. II briefly describes the Kirchoff-Love equation of motion in polar coordinates and the boundary conditions that apply when a circular inclusion made of a different material is embedded in an infinite thin plate. Section III reviews in brief the simplified wave equation developed in Ref. 9 together with the unusual continuity conditions at the boundary of two different media. In Sect. IV the performance of the designed cloak is analyzed in deep using the MLSM, showing that its performance cannot be reproduced using the usual elastic boundary conditions. Afterwards, Sect. V studies the experimentally realized cloak, showing that the numerical simulations based on the MLSM reproduces fairly well the experimental data and characterizes the cloak quality by using the so called averaged visibility. Finally, in section VI the work is summarized and some conclusion are driven.

II. KIRCHOFF-LOVE MODEL FOR A CIRCULAR INCLUSION IN A THIN PLATE

Let us consider the case of flexural (bending) waves propagating in a thin plate with a time harmonic dependence; i.e., $W(\mathbf{r};t) = W(\mathbf{r})e^{-i\omega t}$, where $W(\mathbf{r})$ is the out-of-plane elastic displacement

excited at an arbitrary point **r**. In polar coordinates, $W(\mathbf{r})$ is obtained from the solution of the Kirchhoff-Love wave equation,[16]

$$\frac{\partial^2 M_r}{\partial r^2} - 2\left[\frac{1}{r}\frac{\partial^2 M_{r\theta}}{\partial r\partial\theta} - \frac{1}{r^2}\frac{\partial M_{r\theta}}{\partial\theta}\right] + \left[\frac{1}{r}\frac{\partial^2 M_\theta}{\partial r\partial\theta} + \frac{1}{r^2}\frac{\partial^2 M_\theta}{\partial\theta^2}\right](1) + \rho h\omega^2 W = 0, \tag{1}$$

where

$$M_r = -D\left(\frac{\partial^2 W}{\partial r^2} + \nu\left[\frac{1}{r}\frac{\partial W}{\partial r} + \frac{1}{r^2}\frac{\partial^2 W}{\partial\theta}\right]\right), \tag{2a}$$

$$M_\theta = -D\left(\frac{1}{r}\frac{\partial W}{\partial r} + \frac{1}{r^2}\frac{\partial^2 W}{\partial\theta^2} + \nu\frac{\partial^2 W}{\partial r^2}\right), \tag{2b}$$

$$M_{r\theta} = -D(1-\nu)\left(\frac{1}{r}\frac{\partial^2 W}{\partial r\partial\theta} - \frac{1}{r^2}\frac{\partial W}{\partial\theta}\right), \tag{2c}$$

and $D = Eh^3/12(1-\nu^2)$ is the flexural stiffness, where E is the Young's modulus, ν the Poisson's ratio and h the plate thickness. Finally, ρ defines the mass density of the plate.

Equation (1) indicates that anisotropy in the mass density will not change the equation since ρ is not involved in the partial derivatives. However, introducing anisotropy in either the Young's modulus and/or the Poisson's ratio will create an anisotropic flexural stiffness. Therefore, in an anisotropic medium the partial derivatives over radius and coordinate enter with different coefficients that strongly complicates the dynamical equation.

Now, let us consider that a circular region Ω defined by a certain radius R is located in an infinite homogeneous isotropic thin plate, which is made of a different material. Therefore, the solution to Eq. (1) in polar coordinates is

$$W^-(r,\theta) = W_{inc}(r,\theta) + W_{scat}(r,\theta), \qquad r > R \tag{3a}$$

$$W^+(r,\theta) = W_{int}(r,\theta), \qquad r \le R \tag{3b}$$

where W_{inc}, W_{scat} and W_{int} define the incoming, scattered and internal waves, respectively. It was assumed that the center of the circular region defines the origin of the coordinate axes.

The incoming wave, W_{inc}, is known but the other two should be determined by applying the boundary conditions at the interface Ω. Particularly, the boundary conditions require continuity of the displacement and its derivative over r. In addition, the sum of all radial moments of inertia in M_r and the radial components of the Kirchhoff stress V_r are zero, thus

$$W^-|_\Omega = W^+|_\Omega, \tag{4a}$$

$$\left.\frac{\partial W^-}{\partial r}\right|_\Omega = \left.\frac{W^+}{\partial r}\right|_\Omega, \tag{4b}$$

$$M_r^-|_\Omega = M_r^+|_\Omega, \tag{4c}$$

$$V_r^-|_\Omega = V_r^+|_\Omega, \tag{4d}$$

where V_r is the radial component of the Kirchhoff stress defined as

$$V_r \equiv -D\frac{\partial}{\partial r}(\Delta W) + \frac{\partial}{\partial\theta}M_{r\theta}, \tag{5}$$

where

$$\Delta W = \frac{\partial^2 W}{\partial r^2} + \frac{1}{r}\frac{\partial W}{\partial r} + \frac{1}{r^2}\frac{\partial^2 W}{\partial\theta^2} \tag{6}$$

III. SIMPLIFIED APPROACH

In spite of the extreme complexity expected from Eq. (1) when considering anisotropic plates, Farhat and coworkers[9] arrived to the following simplified wave equation

$$\nabla\cdot\left(\sqrt{\underline{\underline{\zeta}}}\nabla\left[\sqrt{\frac{1}{\rho}}\nabla\cdot\left(\sqrt{\underline{\underline{\zeta}}}\nabla W\right)\right]\right) - \sqrt{\rho}\omega^2 h W = 0, \tag{7}$$

where

$$\underline{\underline{\zeta}} = \left[D_r \hat{r} + D_\theta \hat{\theta} \right], \tag{8}$$

and D_r and D_θ are the radial and angular components of the flexural stiffness, respectively. These components are related to the tensorial Young's modulus $\underline{\underline{E}} = Diag(E_r, E_\theta)$; for example, $D_r = E_r h^3/12(1-\nu^2)$.

A transformation technique was applied to Eq. (7) to obtain the material properties of the cylindrical cloak schematically depicted in Fig. 1. Afterward, the same equation was employed to design a cloak consisting of 10 concentric layers of 6 materials.[17]

Though Eq. (7) is a equation with fourth-order derivatives on W like the Kirchhoff-Love wave equation [see Eq. (1)], substantial differences between them must be pointed out. On the one hand, it is observed that the mass density ρ is inserted between the ∇ differential operators, although in the fundamental wave equation[16] the density appears just as a factor multiplying the plate thickness (h) and the harmonic frequency ω. On the other hand, the tensor defining the flexural stiffness $\underline{\underline{\zeta}}$ depends on two elastic parameters E and ν, but the authors considered that only the Young's modulus is anisotropic. It is also worth mentioning, that the derived wave equation (7) contains square roots of physical magnitudes as constitutive parameters, like the density and the flexural stiffness, a feature that is unusual in standard wave equations.

Let's now consider an homogeneous an isotropic plate of thickness h with flexural stiffness D_0 and density ρ_0. And let's also consider that a circular region Ω with radius R does exist in the plate with different material parameters. Then the solution to Eq. (7) will have the same functional form than that for the Kirchhoff-Love wave equation [see Eq. 1]. In polar coordinates it consists of a linear combination of Bessel functions of the form

$$W^-(r,\theta) = W_{inc}(r,\theta) + W_{scat}(r,\theta) \qquad r > R \tag{9a}$$

$$W^+(r,\theta) = W_{int}(r,\theta) \qquad r \le R \tag{9b}$$

The continuity conditions at the boundary Ω separating the circular region from the surrounding background are obtained by imposing the continuity of the different expressions appearing between parenthesis in Eq. (7). In other words, the boundary conditions are the following

$$W^- = W^+ \tag{10a}$$

$$\hat{r} \cdot \left(\sqrt{D^-} \nabla W^- \right) = \hat{r} \cdot \left(\sqrt{D^+} \nabla W^+ \right) \tag{10b}$$

$$\sqrt{\frac{1}{\rho^-}} \nabla \cdot \left(\sqrt{D^-} \nabla W^- \right) = \sqrt{\frac{1}{\rho^+}} \nabla \cdot \left(\sqrt{D^+} \nabla W^+ \right) \tag{10c}$$

$$\hat{r} \cdot \left(\sqrt{D^-} \nabla \left[\sqrt{\frac{1}{\rho^-}} \nabla \cdot \left(\sqrt{D^-} \nabla W^- \right) \right] \right) = \hat{r} \cdot \left(\sqrt{D^+} \nabla \left[\sqrt{\frac{1}{\rho^+}} \nabla \cdot \left(\sqrt{D^+} \nabla W^+ \right) \right] \right) \tag{10d}$$

where $\hat{r}$ is the unity vector along the radial direction.

These boundary conditions are implicit when one solves Eq. (7) using a numerical solver based on finite elements. Then, by taking into account the boundary Ω between the background and a circular region, they reduce to

$$W^-|_\Omega = W^+|_\Omega \tag{11a}$$

$$\sqrt{D^-} \frac{\partial W^-}{\partial r}\bigg|_\Omega = \sqrt{D^+} \frac{\partial W^+}{\partial r}\bigg|_\Omega \tag{11b}$$

$$\sqrt{\frac{D^-}{\rho^-}} \left(\Delta W^- \right)\bigg|_\Omega = \sqrt{\frac{D^+}{\rho^+}} \left(\Delta W^+ \right)\bigg|_\Omega \tag{11c}$$

$$D^- \sqrt{\frac{1}{\rho^-}} \left(\frac{\partial}{\partial r} \Delta W^- \right)\bigg|_\Omega = D^+ \sqrt{\frac{1}{\rho^+}} \left(\frac{\partial}{\partial r} \Delta W^+ \right)\bigg|_\Omega \tag{11d}$$

Out of these four boundary conditions only the first one has clear physical meaning - continuity of the displacement. The other three do not follow from the standard physical requirements and their physical meaning remains unclear.

IV. THE FLEXURAL CLOAK: A NUMERICAL EXPERIMENT

The flexural cloak designed in Ref. 9 consists of an elastic metamaterial with the following properties

$$D_r = \left(\frac{r-a}{r}\right)^2, \quad D_\theta = \left(\frac{r}{r-a}\right)^2, \tag{12a}$$

$$\rho = \left(\frac{b}{b-a}\right)^4 \left(\frac{r-a}{r}\right)^2, \tag{12b}$$

where the parameters are normalized to their values in the homogeneous plate, D_0 and ρ_0, respectively.

To engineer these metamaterial properties, the authors proposed a binary multilayered radial structure (BMRS) as depicted in Fig. 2.[10] This structure is inspired from the one previously proposed in acoustics to get anisotropic mass density.[3,4] The structure consists of a certain number N of cells, each one consisting of two homogeneous isotropic layers of thicknesses d_A and d_B, flexural stiffnesses D_a and D_b, and densities ρ_A and ρ_B. The homogenization of this structure yields to a metamaterial defined by an anisotropic flexural stiffness and a homogeneous density given by[10]

$$\frac{1}{D_r} = \frac{1}{1+\eta}\left(\frac{1}{D_A} + \frac{\eta}{D_B}\right), \quad D_\theta = \frac{D_A + \eta D_B}{1+\eta}, \tag{13a}$$

$$\rho = \frac{\rho_A + \eta \rho_B}{1+\eta}, \tag{13b}$$

where $\eta = d_B/d_A$ is ratio of thickness of the layers A and B and $d_A + d_B = 1$.

The design can be simplified by considering layers with equal thickness and densities; i.e., $d_A = d_B$ ($\eta = 1$). The resulting cloak consists of alternating layers with the following radially dependent parameters

$$D_A(r) = D_\theta + \sqrt{D_\theta^2 - D_r D_\theta} = \\ = \left(\frac{r}{r-a}\right)^2 + \sqrt{\left(\frac{r}{r-a}\right)^4 - 1}, \tag{14a}$$

$$D_B(r) = D_\theta - \sqrt{D_\theta^2 - D_r D_\theta} = \\ = \left(\frac{r}{r-a}\right)^2 - \sqrt{\left(\frac{r}{r-a}\right)^4 - 1}, \tag{14b}$$

$$\rho_A(r) = \rho_B(r) = \rho(r) = \left(\frac{b}{b-a}\right)^4 \left(\frac{r-a}{r}\right)^2. \tag{14c}$$

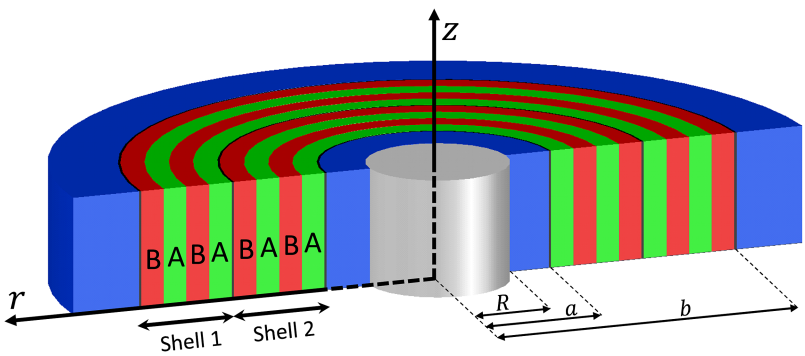

FIG. 2. Scheme of a binary multilayered cloak consisting of just two cells. Each cell is made of four layers; i.e., one pair of AB layers.

Therefore, the cloak consists of alternating layers of high and low flexural stiffness; D_A and D_B respectively.

A. Numerical simulations using the multilayer scattering method

The flexural cloak described above was numerically demonstrated by considering the case of E-shaped rigid clamped object. The cloaking performance is shown in Fig. 1 of Ref. 9.

In this work, however, we employ the multi-layer scattering method (MLSM), which has been already employed to describe the behavior of many devices for flexural waves.[12,13] The MLSM was initially developed for radially dependent acoustic structures,[18] but the method was extended to flexural waves propagating in thin plates containing radially inhomogeneous structures.[12] For a comprehensive description of the MLSM applied to flexural waves the reader is addressed to the Appendix in Ref. 12. In brief, the continuous variation of the parameters is discretized into a number N of homogeneous cylindrical symmetric layers. In each layer n the displacement W_n is a solution of Eq. (1), which in polar coordinates is

$$W_n(r,\theta) = W_n^{(1)}(r,\theta) + W_n^{(2)}(r,\theta) \tag{15}$$

where $W_n^{(1)}(r,\theta)$ and $W_n^{(2)}(r,\theta)$ are solutions of the Helmholtz and Modified Helmholtz equations, respectively. The continuity of the solutions for layer n and layer $n+1$ is guarantee by applying the boundary conditions given in Eqs. (4). To summarize, the MLSM is based in the Kirchoff-Love wave equation and, at the interface of two elastic media, employs the usual boundary conditions described in Sect. II.

The numerical simulations are performed by considering the same values employed in Ref. 9. In particular, we consider an 1 mm thick aluminum plate (h=1 mm) with Young's Modulus $E = 78.97$ GPa, mass density $\rho = 2700$ kg/m^3 and Poisson's ratio $\nu = 0.33$.

The MLSM is specially suitable for dealing with radially symmetrical objects like the acoustic cloak for a clamped cylinder of radius $r = 0.18$ m $< a$. The point source is located at (0.5 m, 0.5 m) and radiates a cylindrical wave of frequency f=1325Hz ($\lambda = 0.28$ m). The shell's geometrical parameters are $a = 0.2$ m and $b = 0.4$ m. The anisotropic shell with thickness $b - a$ is then divided in 25 cells. And each cell consists of two AB pairs (four layers). This is done to ensure that the homogenized anisotropic parameters given in Eqs.(13). Through testing, we concluded that only one AB pair was not enough to obtain the homogenized parameters at a certain distance r from the core center. Overall, there are 100 layers in the shell. The space between the cloak and the clamped region is filled with the background material. A scheme of a cloaking shell made of just two cells (i.e., 4 pairs of AB layers) is shown in Fig. 2

Figure 3 shows the real part (top panel) and the modulus (bottom panel) of the out-of-plane displacement W obtained from the numerical simulations based on the MLSM. It is observed that cloaking is not working and we concluded that results in Ref. 9 cannot be reproduced using the MLSM which employs the usual boundary conditions described in Section I.

However, the results shown in Fig. 1 of Ref. 9 can be reproduced if two modifications are introduced in the MLSM. On the one hand, instead of using the relationship given in Eq. (13) for the homogenization of a BMRS we employ the following ones

$$\frac{1}{\sqrt{D_r}} = \frac{1}{1+\eta}\left(\frac{1}{\sqrt{D_A}} + \frac{\eta}{\sqrt{D_B}}\right), \tag{16a}$$

$$\sqrt{D_\theta} = \frac{\sqrt{D_A} + \eta\sqrt{D_B}}{1+\eta}, \tag{16b}$$

$$\sqrt{\rho} = \frac{\sqrt{\rho_A} + \eta\sqrt{\rho_B}}{1+\eta}. \tag{16c}$$

which are obtained by direct analogy with the acoustic wave equation.

On the other hand, we are also forced to use the unusual boundary conditions described by Eqs.(11), whose physical meaning remains unclear.

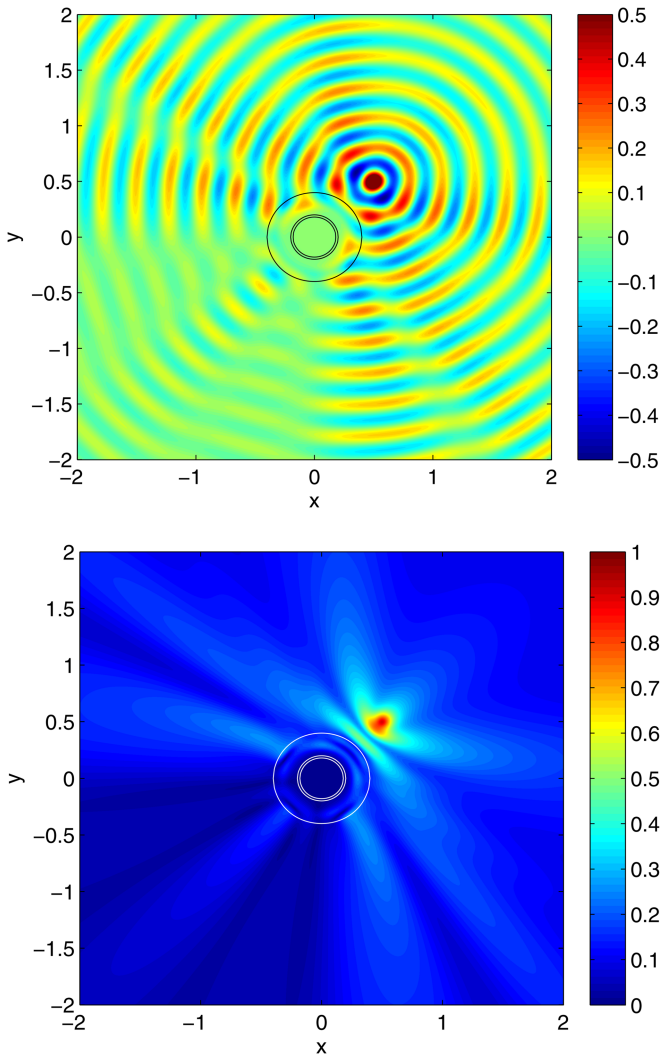

FIG. 3. Real part (top panel) and modulus (bottom panel) of the displacements $W(x,y)$ obtained with the multiple layer scattering method. The punctual source is located at (0.5, 0.5) and the excited vibration interacts with the flexural wave cloak, which in this case is described by the Kirchoff-Love model given in Eqs. (1) to (4). This simulation is unable to reproduce the results shown in Fig. 1 of Ref. 10.

Figure 4 shows the real part (left panel) and the modulus (right panel) of the MLSM numerical simulations using these new set of equations for the BMRS [see Eqs. (16)]and the unusual boundary conditions. Correspondingly, Fig. 5 shows the results for an impinging plane wave with frequency 1325 Hz. It is observed that now the cloaking shell works satisfactorily. The cloaking performance can be even improved by just increasing the number of layers in the BMRS.

The results discussed above indicate that the cloak proposed in Ref. 9 does not work properly when using the MLSM, which is based in the Kirchoff-Love wave equation for flexural waves in thin plates and the usual boundary conditions. We concluded that the cloak performance described in Ref. 9 is associated to an oversimplified wave equation given by Eq. (7), which does not represent a true physical medium. Moreover, this unknown physical medium is accompanied with unusual boundary conditions, which are different to the usual continuity conditions at the interface of two elastic media [see Eqs. (4)].

For a further support of the MLSM, in the following section we will analyzed the flexural cloak engineered by Stenger and coworkers.[11] It will be shown that its experimental characterization is perfectly reproduced by the MLSM.

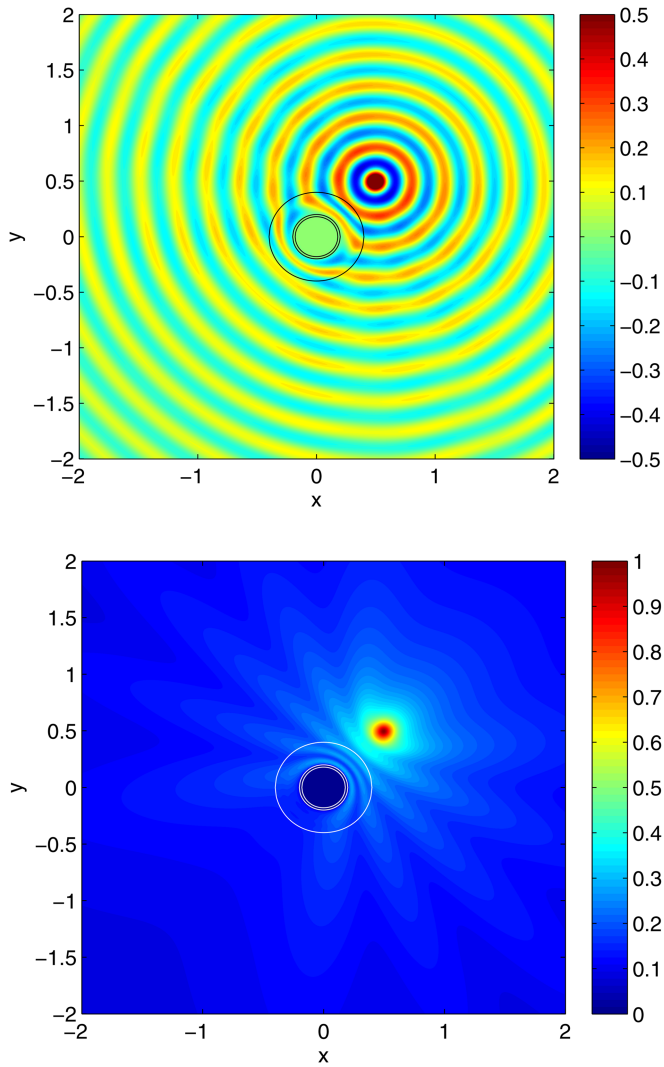

FIG. 4. Real part (top panel) and modulus (bottom panel) of the displacements $W(x,y)$ obtained by using the multilayer scattering method using a cloaking shell consisting of 25 cells, each one consisting of two AB pair of layers. Now the boundary conditions are the ones given in Eqs. (11).

V. A REDUCED FLEXURAL CLOAK: A PRACTICAL DEMONSTRATION

For a practical demonstration of the layered cloak the following reduced set of parameters were proposed[10]

$$D_r^*(r) = \left(\frac{b}{b-a}\right)^4 \left(\frac{r-a}{r}\right)^4, \tag{17a}$$

$$D_\theta^*(r) = \left(\frac{b}{b-a}\right)^4, \tag{17b}$$

$$\rho^* = 1, \tag{17c}$$

which are the result of multiplying Eqs. (14) by the value of ρ.

These anisotropic and inhomogeneous parameters can be obtained by using the BMRS described previously [see Eq. (13)]. The corresponding layers are

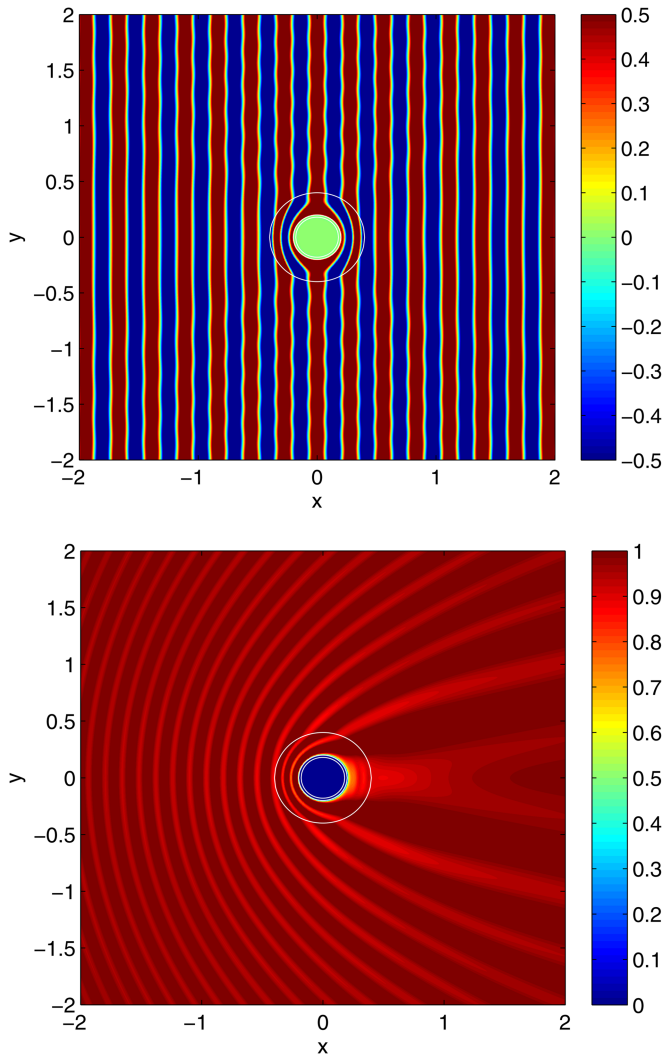

FIG. 5. Behavior of the cloak shown in Fig. 4 interacting with an impinging plane wave of frequency 1325 Hz.

$$D_A^*(r) = \left(\frac{b}{b-a}\right)^4 \left(1 + \sqrt{1 - \left(\frac{r-a}{r}\right)^4}\right), \tag{18a}$$

$$D_B^*(r) = \left(\frac{b}{b-a}\right)^4 \left(1 - \sqrt{1 - \left(\frac{r-a}{r}\right)^4}\right), \tag{18b}$$

$$\rho_A^* = \rho_B^* = 1. \tag{18c}$$

In his work, Stenger *et al.*[11] followed the seminal idea of Farhat *et al.*[10] to design, fabricate and experimentally characterized a cloak for flexural waves propagating in a thin polymer plate. They employed a plate with thickness $h = 1$ mm and a cloaking shell made of 20 concentric layers. Note that instead of using 6 different actual materials as it was proposed, they applied the metamaterial concept for working with just two polymeric materials: polyvinyl chloride (PVC) and polydimethylsiloxane (PDMS). Each concentric layer was fabricated by drilling holes in a PVC plate and filling them with PDMS. So, by changing the filling fraction of the PDMS inclusions they were able to tailor the effective Young modulus of the each layer to the appropriate value. Therefore, they map the continuous reduced parameters of Eq. (17) onto a structure composed of 20 homogeneous and locally isotropic layers. The geometrical description and elastic properties of each layer are reported in Table I. Note that the background layer between the cloak and the clamped core has not been included in the design.

TABLE I. Data values of the 20 homogeneous and locally isotropic layers employed in Ref. 11.

Layer	Radius [mm]	E [Gpa]	ρ[kg/m^3]	ν
Backgr.	> 70	0.5	1100	0.45
1	70.0	2.22	1194	0.45
2	67.0	0.2490	1050	0.45
3	64.5	2.32	1199	0.45
4	61.7	0.2310	1147	0.45
5	59.0	2.01	1186	0.45
6	55.7	0.1710	1038	0.45
7	53.5	2.35	1200	0.45
8	50.6	0.1650	1037	0.45
9	48.0	2.4	1200	0.45
10	45.1	0.1330	1032	0.45
11	42.5	1.84	1174	0.45
12	38.6	0.0631	1018	0.45
13	37.0	1.99	1182	0.45
14	33.4	0.0480	1014	0.45
15	31.5	2.26	1195	0.45
16	28.3	0.03	1010	0.45
17	26.0	2.4	1200	0.45
18	22.9	0.0093	1000	0.45
19	20.5	2.4	1202	0.45
20	17.5	0.0016	1000	0.45
Core	15.0	clamped	clamped	clamped

In order to simulate the measured displacement maps we have employed the MLSM described previously. In brief, the calculations have been performed using the data in Table I and applying the usual boundary conditions at the interface between two elastic media [see Eqs. (4)]. Then, a monochromatic plane wave was injected from the left-hand side and interacts with the object that is clamped in the plate. Afterwards, the calculation is repeated by considering that the object is surrounded by the cloaking shell.

Figure 6 shows several snapshots of the calculated displacements for four impinging frequencies. The left panels show the results corresponding to the isolated clamped object while the right panels correspond to the object with the cloak. It is observed that the calculated maps perfectly reproduce the measured maps reported in Fig. 3 of Ref. 11 for the excitation frequencies of 200, 300, 400 and 450 Hz, respectively. Moreover, the MLSM simulated maps are also in agreement with the calculations reported in Fig. 4 of Ref. 11, which are performed with the commercial software COMSOL MULTIPHYSICS.

The results described above support the quality of the MLSM as an appropriate tool to study radially symmetric structures in thin plates. Moreover, the MLSM practically has the same accuracy than the commercial software based on finite elements but, since it is based on a semi-analytical approach, it allows a better control of the modeling conditions an faster simulation CPU time. Looking at the maps for the modulus, we observe that the scattering of the incident vibration with the clamped region with the cloak produces a reduction of the forward and backwards scattering when they are compared with the case without cloak. We can conclude that, although the cloaking behavior it is not perfect, the cloaking shell is playing its role; it reduces the backward scattering and the shadowing in the forward scattering.

A. Averaged visibility

In order to characterize the performance of the cloak by a single numerical parameter we have calculated the averaged visibility of an object γ, which has been already employed to characterize

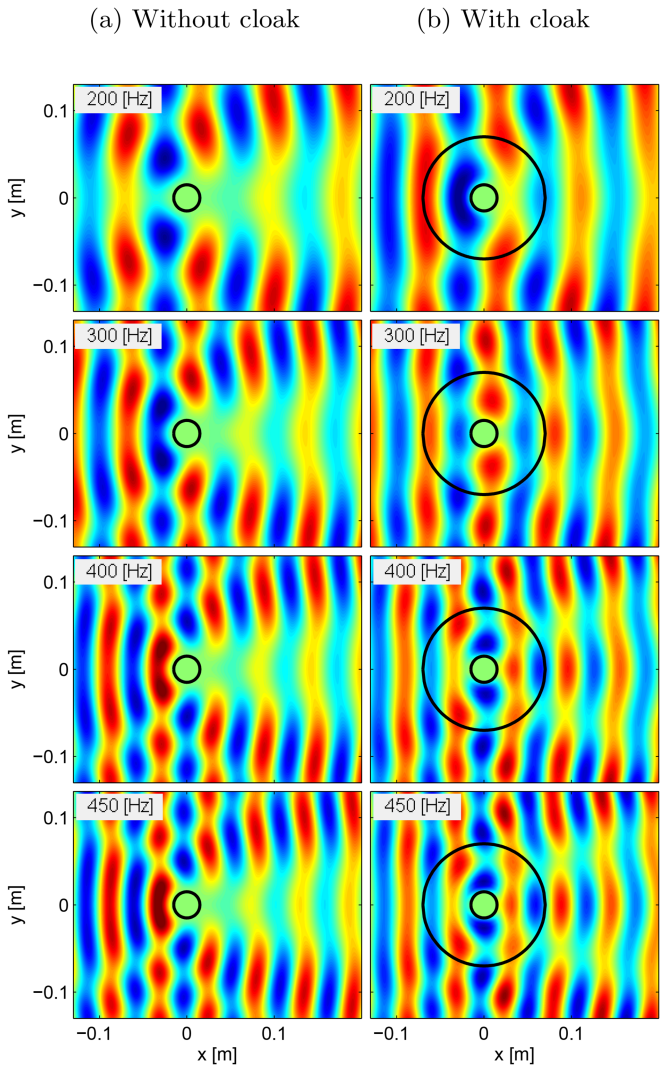

FIG. 6. Calculated snapshots of the displacement map $W(x,y)$ (real part) obtained by using the multilayer scattering simulation method. These results are in excellent agreement with the measurements reported in Fig. 3 of Ref. 11). The left panels (a) corresponds to the homogeneous plate with a clamped circular object (black circle). The right panels (b) corresponds to the object with the cloak The four rows are for excitation frequencies of 200, 300, 400 and 450 Hz. Scale color goes from blue (negative values) to red (positive values).

some reported acoustic cloaks.[6,7,19] Its definition has been extended here to the case of elastic displacements. The reader is addressed to the Appendix in order to get more details on how it is calculated. Remember that γ is specially useful to characterize the fabricated cloaks, where one performs near-field measurements and have a limited field view due to the experimental setup. The averaged visibility substitute the evaluation of the so called scattering cross-sectional area, which is the traditional procedure.

In this work we have calculated the frequency dependence of γ in front and behind the objects in order to evaluate its quality. For each frequency, γ represents the amount of discrepancy between the displacements produced by an object with those in free space. Therefore, from the comparison between γ obtained from the clamped object with that from the object with the cloaking shell we can get a fair estimation of the reduction of scattering and shadowing. A value $\gamma(\omega) = 0$ means that the object has been completely cloaked at that particular frequency.

Figures 7(a) and 7(b) show the frequency dependence of γ calculated in a rectangular area of 7.5 $\times$ 14 cm^2 in front of the cloak and behind the cloak, respectively. Values are obtained every 10 Hz

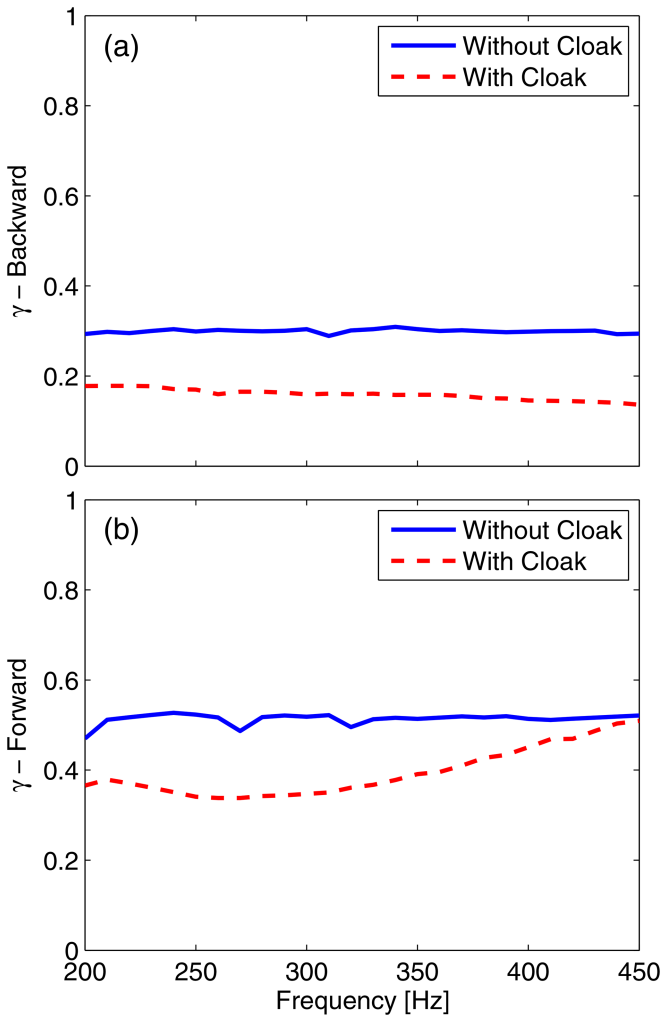

FIG. 7. Averaged visibility (γ) calculated before (a) and after (b) the object for the clamped region without (continuous lines) and with (dashed lines) the cloaking shell proposed by Stenger et al. in Ref. 11.

in the frequency domain between 200 Hz and 450Hz. The comparison with the values obtained for the object without the cloak (continuous lines) indicates a reduction of the averaged visibility due to the cloaking shell. It it shown that the cloak has broadband operation since γ is reduced in the octave band defined from 200 Hz till 400 Hz. The maximum reduction of 35% is achieved in the forward direction, which is obtained at 250 Hz where γ without cloak is 0.52 and with cloak is 0.34. This reduction could be considered modest in comparison with γ values reported for acoustic cloaks. For example, Zhang *et al.*[19] reported a 50% of reduction in the forward direction for their underwater cloak. The experimental cloaks based on scattering cancellation reported measured reductions of 79% and 62%, respectively, for the 2D[6] and 3D[7] cloaking shells.

For the sake of comprehensiveness the Appendix B analyses the flexural wave cloak using the scattering cross-section.

VI. CONCLUSIONS

This work has employed the multilayer scattering method[12,18] to study the flexural wave cloaks proposed by Farhat *et al.*[9] and experimentally realized by Stenger *et al.*[11] The method, which is based on the Kirchoff-love wave equation for flexural waves in thin plates, was unable to reproduce the performance of the theoretically proposed cloak.[9] However, the method reproduces fairly well the

experimental data reported in Ref. 11. An in deep analysis of the results let us to conclude that the fourth-order wave equation employed by Farhat and coworkers in order to design their cloak is an oversimplified approach not representing a true elastic medium as the Kirchhoff-Love wave equation does. Moreover, our analysis demonstrates that the designed cloak does not accomplished the usual boundary conditions at the boundary of two elastic media. The modifications needed to reproduce the cloak performance reported by Farhat and coworkers are here explained and indicate that they correspond to conditions whose physical meaning is unclear.

Regarding the practical demonstration of the flexural wave cloak, our simulations reproduce fairly well the measured displacement maps and support the multilayer scattering method as an excellent tool for characterizing radially symmetric structures. We have verified that the fabricated flexural cloak[11] has broadband operation, in the one octave band between 200 and 400 Hz, and it produces a reduction of the backscattering and shadowing of the out-of-plane vibrations impinging the object with the cloak. However, the calculated reduction of the averaged visibility when the clamped object is surrounded with the cloak can be considered modest in comparison with the reduction of this parameter reported for other fabricated acoustic cloaks.[6,7,19] Therefore, we foresee that new flexural cloaks with better performance should be achieved by improving the design procedure.

ACKNOWLEDGMENTS

This work has been supported by the Spanish Ministerio de Economia y Competitividad and the European Union Fondo Europeo para el Desarrollo Regional (FEDER) under Grant with Ref. TEC2014-53088-C3-1-R. We gratefully acknowledge Nicolas Stenger for providing us the parameters listed in Table I.

APPENDIX A: AVERAGED VISIBILITY

The averaged visibility γ of an object interacting with an incident flexural wave can be defined in terms of the normal displacements W as

$$\gamma = \frac{1}{N}\sum_{j}^{N}\frac{W_{max,j} - W_{min,j}}{W_{max,j} + W_{min,j}}, \tag{A1}$$

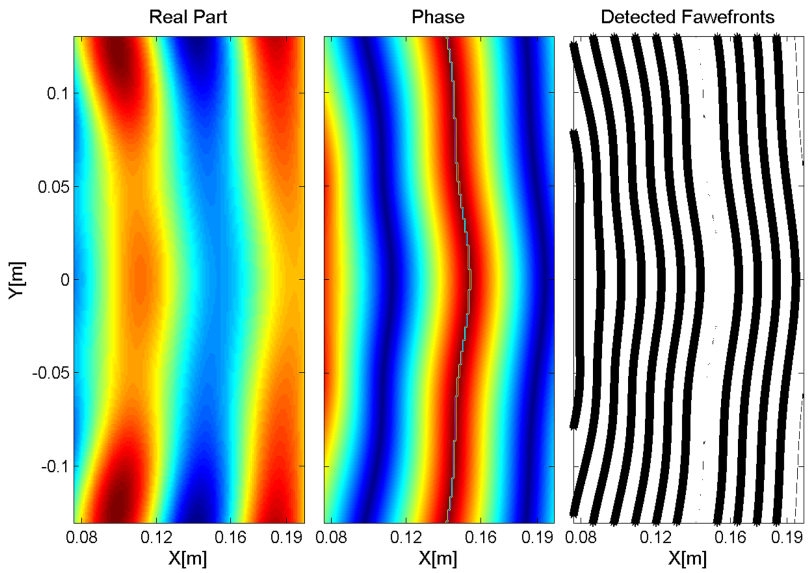

FIG. 8. Snapshots of the calculated displacement map, $W(x, y; \omega)$, using the multilayer scattering method at the frequency of 200 Hz. Real part (left panel), phase (central panel) and detected wavefronts (right panel). The continuous lines in the right panel represent wavefronts with a phase separation of $\pi/4$ radians. One wavefront is barely detected. The depicted area is located in front of the cloak, with 7.5 cm $\leq x \leq$ 20 cm and -13 cm $\leq y \leq$ 13cm.

where N is the number of wavefronts contained in a chosen area and $W_{max,j}$ and $W_{min,j}$ are, respectively, the maximum and minimum displacements inside a given wavefront j. It can be say that γ gives in a single value the discrepancy between the waves scattered from a given object with the waves propagating in free space. Analogous definition has been employed for pressure waves in fluid acoustics, where γ has been calculated to characterize the quality performance of acoustic cloaks.[6,7,19]

Figure 8 summarizes the practical procedure to calculate γ. The right and the center panels show the real part and phase of the out-of-plane displacements $W(x, y; \omega)$, which are depicted in a rectangular area in front of the cloak described in Ref. 11. A frequency of 200 Hz was considered for the impinging wave. The continuous lines in left panel define the wavefronts with a phase separation of $\pi/4$ radians. From this figure it is concluded that eleven wavefronts can be used to calculate γ from Eq. A1 in the chosen area. $N = 11$ is the maximum number of wavefronts that have been employed to determine γ in Figs. 7.

APPENDIX B: SCATTERING CROSS SECTION

A traditional way of characterizing the cloak performance is by studying the scattering cross section (SCS) $\sigma(k, \theta)$.[18]

$$\sigma(k, \theta) = \lim_{r \to \infty} \left| \sqrt{r} W^{scat}(r, \theta; \omega) \right|, \tag{B1}$$

with $\omega = ck$.

The Form Factor (FF) is defined as

$$F(k) = \int_0^{2\pi} |\sigma(k, \theta)|^2 d\theta. \tag{B2}$$

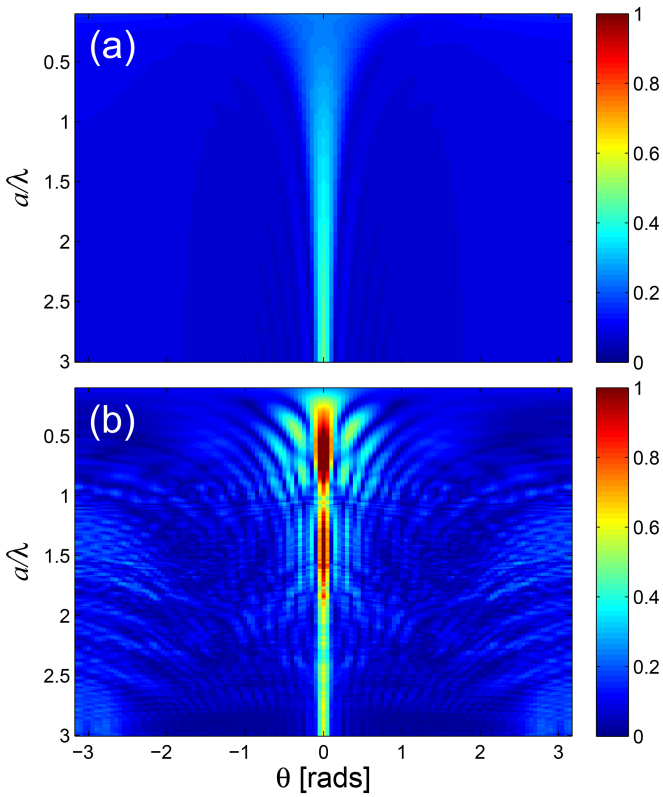

FIG. 9. Angle and frequency dependence of the scattering cross section for the clamped region without (a) and with cloak (b).

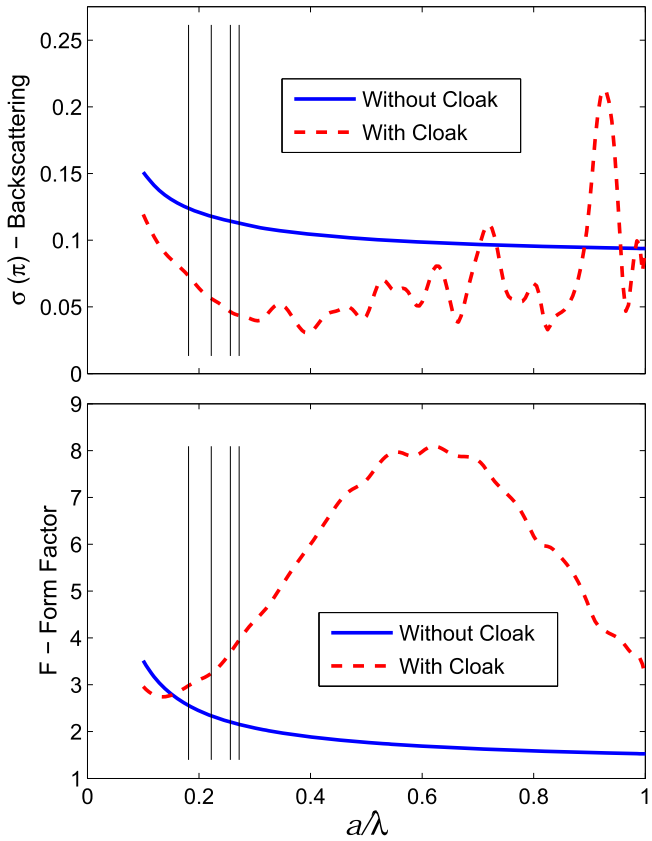

FIG. 10. Frequency dependence of scattering cross section along the back-scattered direction, $\theta = \pi$ (upper panel) and the Form Factor (lower panel) for a clamped circular region without (continuous line) and with cloak (dashed line). The vertical lines are guides for the eye identifying (from left to right) the frequencies 200, 300, 400, 450 Hz, respectively.

This is a single value representing the overall scattering strength of a given scatterer of flexural waves at distances far from the scatterer.

Figures 9(a) and 9(b) shows, respectively, the frequency dependence of the SCS for the clamped region without and with the cloaking shell for a broad range of frequencies (in normalized units) and for all the angles (in radians). The results were obtained by considering $R = a$ in Fig. 1, as described in Ref. 11. It is observed from Fig. 9(a) that the SCS for the bare clumped region - with radius 0.015 m - takes small values for almost all the frequencies and angles. The largest values are obtained along the forward direction ($\theta = \pi$). Figure 9(b) indicates that, when the cloak is added, the SCS increases in all the frequencies and angles due to the larger size of the scatterer, which now has a radius of 0,07 m. The maximum increment is obtained along the forward direction. However, for frequencies below the homogenization limit (i.e., for $\lambda \geq 4a$) the SCS and the FF are similar. In other words, it can be say that, at the far field, the fabricated flexural wave cloak is inefficient for any direction out of the backwards direction. Figure 10 shows the frequency dependence of SCS along the backwards propagation (top panel) and the Form Factor (bottom panel). The vertical lines are guides for the eye corresponding to the measured frequencies (from left to right) of 200, 300, 400 and 450 Hz, respectively. It is observed that the cloaking shell reduces the back-scattering but the starting value is rather low. Regarding the total scattering, which is represented by the FF, it is observed that it is slight larger at the frequencies below the homogenization limit. From these results we can be concluded that the designed cloaking shell is inefficient to reduce the scattering of the flexural waves by the clumped object at distances far from the object. Therefore, the experimental characterization of the SCS and the FF should be considered in future realizations of flexural cloaks.

[1] S. A. Cummer and D. Schurig, New J. Phys. **9**, 45 (2007).
[2] L.-W. Cai and J. Sánchez-Dehesa, New J. Phys. **9**, 450 (2007).
[3] D. Torrent and J. Sánchez-Dehesa, New J. Phys. **10**, 063015 (2008).
[4] Y. Cheng, F. Yang, Y. Xu, and X. Liu, Appl. Phys. Lett. **92**, 151913 (2008).
[5] M. D. Guild, M. Haberman, and A. Alù, J. Acoust. Soc. Am. **99**, 1355 (2011).
[6] V. M. García-Chocano, L. Sanchis, A. Díaz-Rubio, J. Martínez-Pastor, F. Cervera, R. Llopis-Pontiveros, and J. Sánchez-Dehesa, Appl. Phys. Lett. **99**, 074102 (2011).
[7] L. Sanchis, V. M. García-Chocano, R. Llopis-Pontiveros, A. Climente, J. Martínez-Pastor, F. Cervera, and J. Sánchez-Dehesa, Physical Review Letters **110**, 124301 (2013).
[8] M. D. Guild, M. Haberman, and A. Alù, Appl. Phys. Lett. **105**, 023510 (2014).
[9] M. Farhat, S. Guenneau, S. Enoch, and A. Movchan, Physical Review B **79**, 033102 (2009).
[10] M. Farhat, S. Guenneau, and S. Enoch, Phys. Rev. Lett. **103**, 024301 (2009).
[11] N. Stenger, M. Wilhelm, and M. Wegener, Physical Review Letters **108**, 014301 (2012).
[12] A. Climente, D. Torrent, and J. Sánchez-Dehesa, Journal of Applied Physics **114**, 214903 (2013).
[13] A. Climente, D. Torrent, and J. Sánchez-Dehesa, Appl. Phys. Lett. **105**, 064101 (2014).
[14] D. Torrent, Y. Pennec, and B. Djafari-Rouhani, Appl. Phys. Lett. **106**, 224902 (2014).
[15] D. Colquitt, M. Brun, M. Gei, A. Movchan, N. Movchan, and I. Jones, J. Mech. Phys. Solids **72**, 131 (2014).
[16] S. Timoshenko, S. Woinowsky-Krieger, and K. (Firm), *Theory of plates and shells*, 2nd ed. (New York, McGraw-Hill, 1959) includes bibliographical footnote references and indexes.
[17] M. Farhat, S. Guenneanu, and S. Enoch, Phys. Rev. B **85**, 020301 (2012).
[18] L.-W. Cai and J. Sánchez-Dehesa, The Journal of the Acoustical Society of America **124**, 2715 (2008).
[19] S. Zhang, C. Xia, and N. Fang, Physical Review Letters **106**, 024301 (2011).